ACS APPLIED MATERIALS & INTERFACES

RESEARCH ARTICLE

www.acsami.org

Superhard Tungsten Tetraboride Films Prepared by Pulsed Laser Deposition Method

Julietta V. Rau,[†,*] Alessandro Latini,[‡] Roberto Teghil,[§] Angela De Bonis,[§] Marco Fosca,[†] Ruggero Caminiti,[‡] and Valerio Rossi Albertini[†]

[†]Istituto di Struttura della Materia, Consiglio Nazionale delle Ricerche (CNR), Via del Fosso del Cavaliere, 100-00133, Rome, Italy

[‡]Università di Roma "La Sapienza", Dipartimento di Chimica, Piazzale Aldo Moro, 5-00185 Rome, Italy

[§]Università della Basilicata, Dipartimento di Chimica "A.M. Tamburro", Via dell'Ateneo Lucano 10-85100 Potenza, Italy; CNR-IMIP UOS di Potenza, Zona Industriale di Tito scalo (PZ), Italy

ABSTRACT: Attempts to synthesize and/or theoretically predict new superhard materials are the subject of an intense research activity. The trials to deposit them in the form of films have just began. WB_2 (77 wt % WB_2 and 23 wt % WB_4) and WB_4 (65 wt % WB_4 and 35 wt % WB_2) polycrystalline bulk samples were obtained in this work via electron beam synthesis technique and, subsequently, used as targets for films preparation by the pulsed laser deposition method. The targets were irradiated by a frequency-doubled Nd:glass laser with a pulse duration of 250 fs. The films grown on SiO_2 substrates at 600 °C were characterized by X-ray diffraction, scanning electron and atomic force microscopies, and Vickers microhardness technique. The deposited films are composed of WB_4. The intrinsic film hardness, calculated according to the "law-of-mixtures" model, lies in the superhardness region 42−50 GPa.

KEYWORDS: tungsten diboride, tungsten tetraboride, tungsten tetraboride film, hardness, superhard, pulsed laser deposition

1. INTRODUCTION

A great interest is currently focused on the synthesis of superhard materials, i.e., those possessing Vickers hardness ≥40 GPa (this value being imposed by convention). This interest is motivated by the technological requirements and the need for physically and chemically resistant materials for cutting tools and wear resistant coatings, overcoming the technological limits of applicability of diamond and cubic boron nitride, used for processing and polishing of the iron-based alloys. Superhard coatings have also promising technical capabilities for the application in the defense and aerospace industries. Moreover, tungsten boride films can be used as diffusion barriers.[1] Several approaches were proposed recently to be employed in the development of this new class of materials,[2−4] the goal being not to create a material harder than diamond but, rather, to engineer a material that is both superhard and can be easily synthesized in bulk quantities, avoiding the use of high pressure.[5] Following these strategies, several new superhard materials were synthesized, such as some transition metal borides, ReB_2,[6,7] and $IrB_{1.35}$.[7] Other candidates for superhardness, such as OsB_2,[8] RuB_2,[7] and $RhB_{1.1}$,[7] were found to be hard.

Very recently, theoretical calculations based on structural, elastic, and electronic properties predicted WB_2[9,10] and WB_4[11] to be potential candidates for ultraincompressible and hard materials, and therefore of advanced fundamental and technological interest.

As to the corresponding films, very few studies dedicated to the coatings deposition have been performed up to now. The available literature data (our earlier works) regard deposition of ReB_2,[12] RuB_2−Ru_2B_3,[13] $IrB_{1.1}$, and $RhB_{1.1}$[14] coatings, all of them being superhard and produced by ultrashort (femtosecond) pulsed laser deposition technique. To the best of our knowledge, there are only a few more literature references[1,15] that apply to obtaining the coatings of this class of materials. In a recent work,[15] the authors used a pulsed free electron laser IR beam for a confined-plume chemical deposition synthesis and reported on the preparation of the microcrystalline WB_4 coatings. In ref 1, r.f. magnetron sputtering deposition of amorphous tungsten boride films, with the so-called WB_x composition, is reported.

In this paper, we present a study dedicated to the possibility to deposit WB_4 films, applying the same deposition approach (femtosecond PLD) followed in our earlier works,[12−14] which has been proved to be successful. The films properties were investigated by X-ray Diffraction (XRD), scanning electron microscopy−energy-dispersive X-ray spectroscopy (SEM-EDS), atomic force microscopy (AFM), and Vickers microhardness techniques.

2. EXPERIMENTAL SECTION

2.1. Synthesis of Tungsten Boride Targets. Tungsten boride targets were synthesized applying an electron beam synthesis technique, the details of which can be found elsewhere.[16] In brief, tungsten powder (Alfa Aesar, APS 1−5 μm, purity 99.9%) and crystalline boron powder (Alfa Aesar, ∼60 mesh, purity 99.5%) in the molar ratio of 1:2.5 and 1:4.5 for the WB_2 and WB_4 targets, respectively (in order to compensate the evaporative loss of boron during the synthesis, because its vapor pressure is sensibly higher than that of tungsten in all the functional temperature range[17]), were carefully mixed in an agate mortar with the addition of some acetone to facilitate intimate mixing. After the mixing procedure and drying of the powders, the mixtures were cold-pressed

Received: July 15, 2011
Accepted: August 30, 2011
Published: August 30, 2011

into pellets (diameter 18 mm). The pellets, contained in TiB_2/BN composite crucibles (GE Advanced Ceramics, UK), were positioned into the pocket of an electron beam gun (model EV1−8, Ferrotec, Germany) inside a high vacuum chamber evacuated by a turbo pump. Each pellet was melted two times (the second melting was performed after repositioning the pellet upside-down), so to ensure the completeness of the reaction. The pressure inside the chamber during the synthesis was $\sim 1 \times 10^{-6}$ mbar. For the melting process, an accelerating voltage of the electron beam of −3.5 kV and an emission current in the range of 30−150 mA were used.

2.2. Pulsed Laser Deposition of Films. WB_4 films were deposited on the amorphous SiO_2 substrates (1 mm thick fused silica slides) by means of the pulsed laser deposition technique. PLD utilizes a pulsed laser radiation for evaporating, in a vacuum chamber, of a solid target. Then, the expanding evaporated material is deposited on the surface of a suitable substrate to form a film. PLD is a versatile deposition technique, particularly well suited to grow thin films of a large number of materials with technological interest, such as nitrides, carbides, and borides. This technique has been widely used for its capability to evaporate and to deposit refractory materials, transferring the target stoichiometry to the film.[18]

The deposition experiments were performed in a multiport stainless steel vacuum chamber, evacuated by a rotary-turbomolecular pumping system. The working pressure was 4×10^{-4} Pa. The chamber was equipped with a support for the target to minimize craterisation effects, quartz windows for the inlet of the laser beam and a substrate holder, resistively heated. The ablation laser source was a frequency-doubled Nd:glass laser (light conversion, λ = 527 nm, pulse duration 250 fs, repetition rate 10 Hz, E = 2.7 mJ). The laser beam, focused by a suitable optical system, was oriented with an inclination angle of 45° with respect to the target surface, the spot area being 0.1 mm^2. The substrate and target were assembled in a frontal geometry at 2 cm of reciprocal distance. The deposition time was 4 h. The substrate temperature was kept at 600 °C.

2.3. X-ray Diffraction Analysis. The tungsten boride targets and films were analyzed using a Panalytical X'Pert Pro diffractometer (Bragg−Brentano geometry, CuK_α radiation, λ = 1.54184 Å), equipped with powder and thin film (parallel beam) optics. Both optics use a gas filled proportional detector. For powder analyses, pieces of the electron beam synthesized materials were grinded in a steel mortar in order to obtain fine powders, suitable for diffraction analysis. For the powder samples obtained from the targets, $\theta-\theta$ scans were performed, using an incident beam slit of 1°, coupled with a 10 mm mask, a collimator of 0.04 rad and a Ni filter for the Kβ component of the Cu radiation. For the films, 2θ scans were performed, with a fixed incident beam angle of 2° for the film obtained from the WB_4 target and of 3° for the film obtained from the WB_2 target. This type of scan is preferred for thin films in order to suppress the substrate contribution to the diffraction patterns. In this case, an incident beam slit of 0.03125° coupled with a 20 mm mask and a collimator of 0.04 rad were used, while the Ni filter in this case is not necessary, because the thin film optics is equipped with a graphite monochromator on the detector arm. The diffraction patterns were collected in the angular range of 20−90°. Once collected, the diffractograms of the powders were analyzed using the MAUD Rietveld software package. From the Rietveld method, phase composition and refined unit-cell parameters were obtained. The Rietveld refinement was not possible in the case of films because of the low intensity of the diffraction peaks. In this cases, only crystallite size estimation was performed by making use of the Scherrer equation, the instrumental broadening being of 0.1°.

2.4. Scanning Electron Microscopy Morphological Studies. A SEM apparatus (a LEO 1450 variable pressure), working in secondary and backscattered electron modes, with a resolution of about 4 nm in vacuum conditions, was utilized for morphological studies of the deposited tungsten tetraboride films on the SiO_2 substrates. The SEM apparatus was coupled with a system for EDS (energy-dispersive X-ray spectroscopy) microanalysis INCA 300, allowing to execute qualitative/quantitative analysis of the elements. For morphological investigation, the film samples were coated with an ultrathin gold layer. The plane and cross section view images were obtained, the latter being necessary for the thickness measurements. Since the images of the films thickness were obtained at the sample edge tilted by 45 degrees, the measured values were multiplied by $\sqrt{2}/2$. The thickness measurements were carried out in the backscattered electron mode by means of the 4 quadrants detector. The atomic number contrast, presented in the SEM images as gray color hues, allowed to precisely distinguish the film boundary and the interface with the SiO_2 substrate. To confirm the results of the atomic number contrast, we have carried out the EDS analysis of the chemical nature of the observed phases.

2.5. Atomic Force Microscopy Topographical Studies. A noncommercial atomic force microscope was used to investigate the surface texture of the deposited films in a noncontact mode. At first, several portions of the samples were observed to evaluate the homogeneity of the film growth, and, subsequently, high-resolution topographies (3 × 3 μm, 400 points/line) were collected to obtain the quantitative information about the surface fine morphology.

2.6. Vickers Microhardness Measurements. The microhardness measurements were carried out by means of a Leica VMHT apparatus (Leica GmbH, Germany), equipped with a standard Vickers pyramidal indenter (square-based diamond pyramid of 136° face angle). The loading and unloading speed was 5×10^{-6} m/s, and the time under the load was 15 s.

For film samples, the measured hardness was that of the film/substrate composite system. To separate the composite hardness of the film/substrate system (H_c) into its components, film (H_f) and substrate (H_s), we applied a Jönsson and Hogmark "law-of-mixtures" model.[19] In this case, composite hardness H_c of the film−substrate system is expressed as

$$H_c = (A_f/A)H_f + (A_s/A)H_s \quad (1)$$

where A is total contact area; H is the hardness; subscripts f and s denote film and substrate, respectively; $A = A_f + A_s$ is the total contact area. From geometric considerations, eq 1 can be expressed as follows[20]

$$H_f = H_s + (H_c - H_s)/[2c(t/d) - c^2(t/d)^2] \quad (2)$$

where $c = 2\sin^2 11° \approx 0.07$ for hard brittle film on softer substrate, t is film thickness, $d \approx (1/7)D$ is the indentation depth, and D is the imprint diagonal. Furthermore, the indentation size effect (ISE) was taken into account.[21,22] A reasonable expression for the H_c, based on the "law-of-mixtures" approach and accounting for ISE, is

$$H_c = H_{s0} + [B_s + 2c_1 t(H_{f0} - H_{s0})]/D \quad (3)$$

where $c_1 = c(D/d) \approx 0.5$; H_{f0} and H_{s0} are intrinsic hardness of the film and substrate; B_s is a coefficient, which can be determined from a separate experiment on hardness of the substrate, and D is the imprint diagonal.

To evaluate H_{s0} and B_s values, the hardness of the SiO_2 substrate was measured. The relation between the measured substrate hardness, H_s, and the reciprocal length of the indentation imprints is expressed by the following equation

$$H_s = H_{s0} + B_s/D \quad (4)$$

The values obtained for the SiO_2 substrate, H_{s0} and the B_s coefficient, are equal to 5.8 ± 0.7 GPa and $(61.7 \pm 9.5) \times 10^{-6}$ GPa m, respectively.

To calculate the intrinsic hardness of films, special attention was paid to correctly choose the indentation depths, d=D/7 (for Vickers pyramidal indenter), i.e. the range, where the applied model is valid.

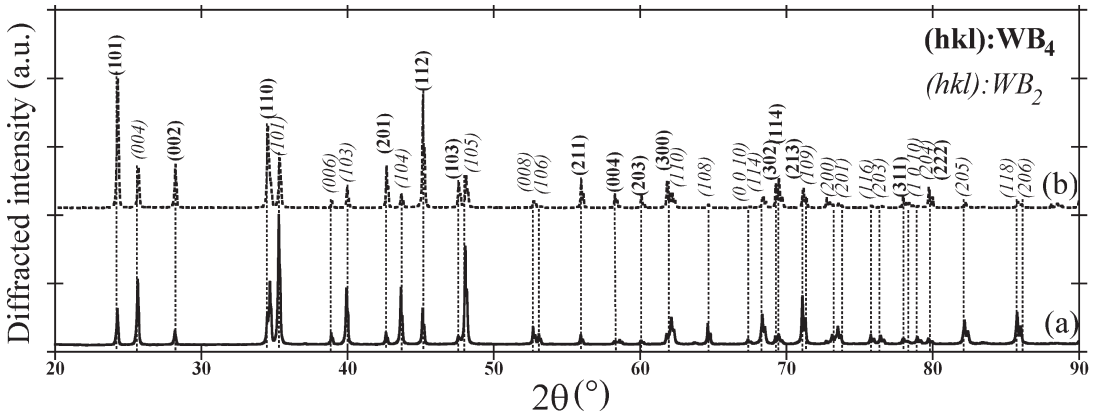

Figure 1. X-ray powder diffraction pattern of (a) WB_2 (77 wt %) (target 1); (b) WB_4 (65 wt %) (target 2).

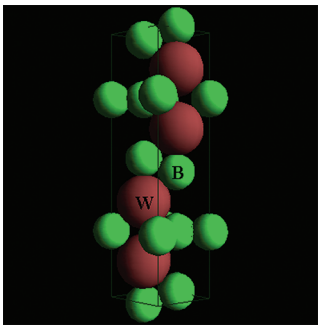

Figure 2. WB_2 hexagonal crystal structure.

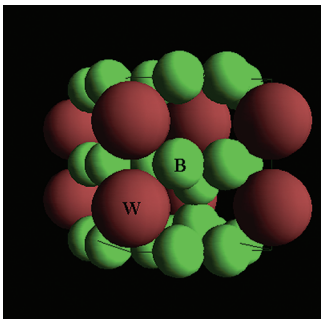

Figure 3. WB_4 hexagonal crystal structure.

The $d/t = D/7t$ range for the films deposited on SiO_2 substrates was (0.5−5.7), perfectly in the range of the substrate-dominated mixed region, where the film is fractured conforming to the plastically deforming substrate.[20]

For hardness measurements on bulk and on the film/substrate systems, indentations were made, applying 5−7 loads ranging from 0.15 up to 9.80 N. To get better statistics, were randomly performed approximately 10−15 indentations at each load.

3. RESULTS AND DISCUSSION

In the works of Brazhkin[2] and Kaner,[3] WB_2 and WB_4 were claimed to be good candidates for superhardness. However, there is not so much known about the mechanical properties of WB_2 and WB_4, likely because of the difficulties in synthesizing the single phase bulk. Indeed, we met the same difficulties during the bulk synthesis procedure.

Diffractograms a and b reported in Figure 1 refer to the WB_2 and WB_4 bulk targets, respectively. The diffractograms clearly show that in both cases, no pure phases were obtained. The targets are both biphasic, containing peaks of WB_2 and WB_4. The composition of the targets, calculated based on the Rietveld refinement, is the following (in wt %):

- WB_2 target (mixed phase, further called target 1): 77 ± 1% WB_2 and 23 ± 1% WB_4.
- WB_4 target (mixed phase, further called target 2): 65 ± 1% WB_4 and 35 ± 1% WB_2.

No free tungsten and/or boron were detected. This phenomenon, in the case of the target 2, can be attributed to the exceedingly high difference of vapor pressure between the two elements during the melting process (~1×10^{-1} Pa for W vs ~1×10^{3} Pa for B at 3000 °C[17]), so that a molar excess of B (12.5%) is not sufficient to ensure the WB_4 stoichiometry in the final product. On the other side, it is not clear why, in the case of the target 1, the same behavior is not observed.

WB_2 and WB_4 phases both possess hexagonal crystal structure (Figures 2 and 3, respectively) (space group $P6_3/mmc$ for both. For WB_2 a = 2.9831 Å and c = 13.879 Å (card number 73−1244);[23] for WB_4 a = 5.200 Å and c = 6.340 Å (card number 19−1373).[23] The refined structural parameters obtained in this work for the targets are

- target 1: for the WB_2 phase a = 2.986 ± 0.001 Å, c = 13.891 ± 0.001 Å; for the WB_4 phase a = 5.198 ± 0.001 Å and c = 6.331 ± 0.001 Å.
- target 2: for the WB_2 phase a = 2.985 ± 0.001 Å, c = 13.889 ± 0.001 Å; for the WB_4 phase a = 5.198 ± 0.001 Å and c = 6.334 ± 0.001 Å.

The agreement with the reference literature data is excellent. In both cases, the crystallite size is in the micrometer range, and the rms microstrain is not significant.

The diffractograms reported in Figure 4 (a and b) refer to the films obtained from the target 1 and 2, respectively. As stated in the experimental section, the Rietveld refinement procedure was not possible, so only a phase analysis by the fingerprint method and an estimation of the crystallite sizes using the Scherrer equation were carried out. The phase analysis of the diffractogram, presented in Figure 4(a), revealed that the film obtained from the target 1 is composed mainly of WB_4. However, some unidentified peaks can be observed on the diffractogram, indicated with asterisc*. Whereas, the film obtained from the target 2 is composed of phase pure WB_4 (Figure 4(b)).

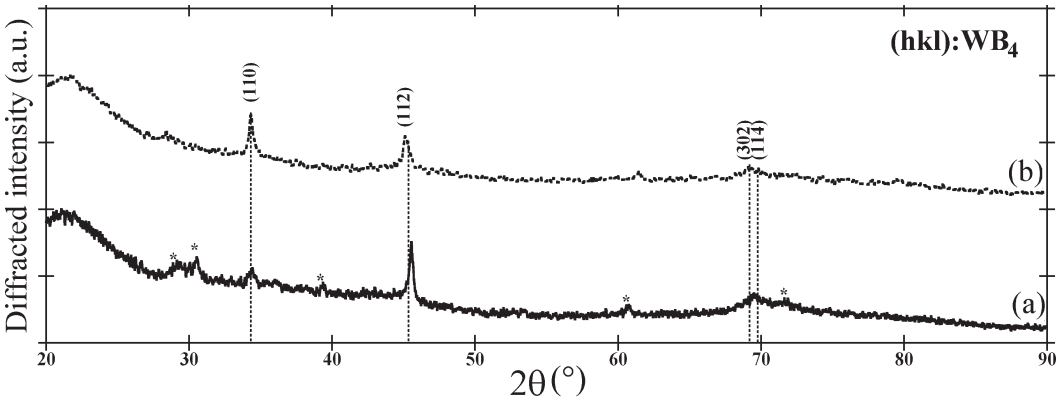

Figure 4. X-ray powder diffraction pattern of (a) WB_4 film deposited from target 1; (b) WB_4 film deposited from target 2.

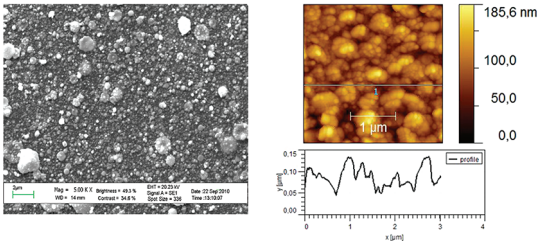

Figure 5. SEM micrograph (left) and AFM image (right) of WB_4 film deposited from target 1.

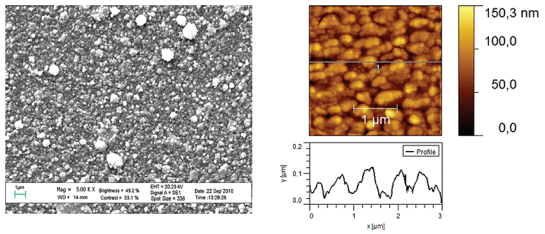

Figure 6. SEM micrograph (left) and AFM image (right) of WB_4 film deposited from target 2.

The Scherrer equation gives an estimated average crystallite size of about 40 nm (obviously for the WB_4 phase) for the film obtained from the target 1, and of about 30 nm for the film deposited from the target 2.

The film morphology was investigated by SEM. SEM images of films deposited from the target 1 and 2 at 5000× magnification are presented in Figures 5 and 6 (left), respectively. From the SEM plane view images, it can be seen that both the films exhibit a similar morphology, the films surface having a dense globular grain texture. It should be noted that the morphology of the WB_4 films is very similar to that of the $RhB_{1.1}$ and $IrB_{1.1}$ films and of the ReB_2 and $RuB_2-Ru_2B_3$ films reported by us previously.[12,13] All these coatings were produced in the same way, applying pulsed laser deposition technique and the femtosecond laser source. The film deposited from the target 2 seems to have a more homogeneous distribution of the grain size (see Figure 6-(left)), being in the submicrometer range (300−400 nm).

According to the SEM-EDS data, the W/B atomic ratio in the films is close to its stoichiometric ratio of 1:4, somewhat less boron amount being registered in the case of film deposited from the target 1. The film thickness was estimated from the cross-section SEM images, being about 0.8 ± 0.1 μm.

The topography of the films surface was examined by AFM. Several AFM images were acquired in the noncontact mode, in order to characterize the surface. In Figures 5 and 6 (right), two examples of topographic images, clearly showing the globular films texture, are presented. These results evidence a more homogeneously textured surface for the film deposited from the target 2 (Figure 6 (right)), in agreement with the results obtained by SEM. From the AFM images, as well as from the SEM ones, appear that both the films are composed of submicrometer size grains. Moreover, from the AFM images, it is visible that large submicrometer grains exhibit a substructure, i.e., are composed of smaller particles.

From the XRD analysis, it turns out that the films are nanostructured and composed of small grains: about 40 nm of the average grain size for the film obtained from the target 1, and about 30 nm for the film obtained from the target 2. It is worth noticing that because the peak broadening in XRD is dominated by small crystallites, this result does not contradict the results obtained by SEM and is in agreement with the results obtained by AFM. Therefore, one might conclude that the grain size distribution range is rather broad.

The average surface roughness (rms) (quantified by the vertical deviations of the real surface from the ideal surface plane), calculated for these coatings from the AFM images, is 26.7 ± 0.5 nm for the WB_4 film grown from the target 1, and 21.1 ± 0.5 nm for the WB_4 film grown from the target 2. No significant difference in the surface topography between the films can be observed.

As to the hardness of tungsten borides bulk, according to theoretical calculations, Vickers hardness of WB_2 should be similar to that of the superhard ReB_2. The authors[10] obtained for WB_2 the Vickers hardness of about 47 GPa, using the calculated shear moduli. This theoretical WB_2 hardness is considerably higher than that measured by Okada et al[24] (21.3 ± 0.4 GPa). However, it should be noted that Okada's samples were of a defective W_2B_5-type structure (but not of the ideal ReB_2-type) and contained less boron than that corresponding to the chemical formula. Indeed, other literature data also report a hardness decrease due to the boron-deficient network.[5]

According to Gu,[25] the WB_2 hardness under the applied load of 0.49 N is equal to 38.4 ± 1.4 GPa (lower than that of WB_4), whereas its load-independent hardness is 27.7 ± 0.6 GPa.

Table 1. Experimental Data on Vickers Hardness of WB_2 (77 wt %) Bulk (target 1)

	no. of points	applied load (N)	D avg (μm)	H_v avg (GPa)
1	10	0.49	4.7 ± 0.4	42.2 ± 7.0
2	10	0.98	7.4 ± 0.4	33.8 ± 3.5
3	10	1.96	12.8 ± 0.4	22.7 ± 1.6
4	10	2.94	16.5 ± 0.8	20.6 ± 2.0
5	11	4.90	23.0 ± 1.3	17.7 ± 2.0

Table 2. Experimental Data on Vickers Hardness of WB_4 (65 wt %) Bulk (target 2)

	no. of points	applied load (N)	D avg (μm)	H_v avg (GPa)
1	11	0.49	3.8 ± 0.3	65.3 ± 8.5
2	10	0.98	6.2 ± 0.4	48.9 ± 7.0
3	10	1.96	10.8 ± 0.6	32.0 ± 3.3
4	10	2.94	13.9 ± 0.8	29.2 ± 3.6
5	11	4.90	19.3 ± 1.6	25.4 ± 4.4
6	11	9.80	29.8 ± 2.0	21.2 ± 2.8

In this work, WB_2 bulk samples (target 1) were tested with microindentation technique at various loads to determine the Vickers hardness, and the results are presented in Table 1. As the load was increased from 0.49 up to 4.90 N, the average hardness decreased from 42.2 down to 17.7 GPa. As can be seen, a maximum hardness of 42.2 GPa was measured under the low load (0.49 N), whereas the load-independent asymptotic average hardness is about 20 ± 2 GPa.

In ref 11, it is suggested that the WB_4 compound is superhard, on the basis of theoretical first-principles calculations, and its Vickers hardness exceeds the threshold value of 40 GPa. Such a high hardness, according to that work, can be explained by the unique structure of this compound, namely, by a three-dimensional B−B covalent bonding network, consisting of *xy* planar honeycomb B lattice and of a peculiar B_2 dimer along the *z*-axis (see Figure 3).

Brazhkin[2] claimed for both WB_2 and WB_4 the very high hardness of 36−40 GPa. Recently, Gu et al.[25] synthesized WB_4 via arc-melting and measured its mechanical properties, reporting an average Vickers hardness value of 46.2 ± 1.2 GPa under the applied load of 0.49 N, which was confirmed by Mohammadi et al.,[26] whereas its load-independent hardness was found to be about 31.8 ± 1.2 GPa. Gu et al.[25] demonstrated that WB_4 scratches dimond surface, as ReB_2 does.[5]

In this work, we obtained even a higher hardness for WB_4 (65.3 GPa), compared to that reported by Gu[25] under the same load (0.49 N) (see Table 2). WB_4 bulk samples (target 2) were tested with the microindentation technique at various loads to determine the Vickers hardness. A maximum hardness was measured under the load of 0.49 N (65.3 GPa). It decreased, as the load was increased, down to a value of 21.2 GPa under the load of 9.80 N, whereas the load-independent asymptotic average hardness is about 25 ± 2 GPa.

Generally, at low loads, the hardness of many materials exhibits a strong dependence on the load, increasing as the load decreases, this effect being known as the indentation size effect. If we consider the hardness values obtained at low load (0.49 N) only, both the WB_2 and WB_4 mixed phase materials are superhard (see Tables 1 and 2). Instead, several authors suppose that the hardness, obtained from the asymptotic load-independent region, is more meaningful to compare the hardness of materials.[2,27]

Table 3. Experimental Data on Vickers Hardness for WB_4 Film on SiO_2 Substrate Deposited from Target 1

	no. of points	applied load (N)	D avg (μm)	H_c avg (GPa)
1	11	0.147	2.6 ± 0.4	39.3 ± 5.1
2	10	0.245	4.3 ± 0.2	25.7 ± 2.7
3	11	0.490	8.5 ± 0.4	13.0 ± 1.2
4	10	0.981	12.8 ± 0.4	11.4 ± 0.8
5	10	1.961	18.9 ± 0.8	10.4 ± 0.9
6	15	2.942	23.7 ± 1.2	10.0 ± 1.0
7	15	4.903	31.8 ± 1.3	9.5 ± 1.0

Table 4. Experimental Data on Vickers Hardness for WB_4 Film on SiO_2 Substrate Deposited from Target 2

	no. of points	applied load (N)	D average (μm)	H_c average (GPa)
1	12	0.147	2.6 ± 0.1	40.7 ± 3.3
2	10	0.245	3.6 ± 0.1	35.8 ± 3.0
3	15	0.490	8.0 ± 0.4	14.6 ± 1.4
4	12	0.981	11.4 ± 0.5	14.3 ± 1.3
5	14	1.961	19.3 ± 0.5	10.0 ± 0.5
6	15	2.942	23.6 ± 0.4	10.0 ± 0.3
7	15	4.903	32.1 ± 1.6	9.0 ± 0.9

Table 5. Vickers Microhardness and Thickness of WB_4 Films and Microhardness of Corresponding Bulk Borides

film	intrinsic film hardness, H_{f0} (GPa)
WB_2 bulk (target 1)	20 ± 2
WB_4 film from target 1	42 ± 5
WB_4 bulk (target 2)	25 ± 2
WB_4 film from target 2	50 ± 6

The hardness is known to increase with the increase of B content,[25] which explains why WB_4 is harder than WB_2.

Our Vickers hardness data are representative of the average hardness for all the crystallographic planes of polycrystalline WB_2 and WB_4 bulk samples. This point should be taken into account while comparing the hardness data from various literature sources. For example, in ref 28, the results for full elastic tensor of three different forms of ReB_2, two isotropic polycrystalline specimens and one hexagonal symmetry highly oriented grain specimen, are reported. The measured moduli of the ReB_2 grain-oriented crystal exceed the corresponding values for the polycrystal. Furthermore, hardness, like other mechanical properties, generally depends on the macroscopic characteristics of materials (morphology, presence of defects, admixtures, possible imhomogeneities etc.). The authors[28] also concluded that the measured moduli are strongly dependent on the morphology of the samples and on the presence of an excess of boron.

For ReB_2, for instance, the addition of 0.5 mols of excess of amorphous boron during its synthesis, led to a substantial decrease of hardness. Although the additional boron produces

a phase pure product, according to the X-ray diffraction analysis, the boron excess distributed through the bulk drastically reduces the hardness of material.[5]

For coatings, the obtained experimental data for the composite film/substrate hardness of the WB_4 films deposited on the SiO_2 substrates are presented in Tables 3 and 4, respectively. Calculated intrinsic hardness values for the films, obtained from these data, are summarized in Table 5.

As it can be seen from Table 5, both the films are superhard. It is known that many materials exhibit an increase in hardness, when deposited as a film in comparison with the bulk material.[29] This enhancement involves a complex interaction of several factors, leading to the decrease in dislocation mobility, such as grain size decrease, grain boundaries densification and compressive stress, as the result of deposition process.

4. CONCLUSIONS

The WB_4 films were prepared by the Pulsed Laser Deposition technique, utilizing a femtosecond laser source. The films exhibit a dense globular grain texture. The distribution of the grain size is broad. The Scherrer equation gives an average grain size of about 30−40 nm, confirmed by AFM, while the SEM results suggest that the films are composed of submicrometer grains. The average surface roughness is in the range of 21−27 nm. The deposited WB_4 films are 0.8 ± 0.1 μm thick, and the intrinsic film hardness is high, in the range of 42−50 GPa.

AUTHOR INFORMATION

Corresponding Author

*Tel: +39-06-4993 4086. Fax: +39-06-4993 4153. E-mail: giulietta.rau@ism.cnr.it.

ACKNOWLEDGMENT

The authors thank Dr. D. Ferro for performing SEM-EDS measurements.

REFERENCES

(1) Willer, J.; Pompl, S.; Ristow, D.; Siemens, A. G. *Thin Solid Films* **1990**, *188*, 157–163.
(2) Brazhkin, V. V.; Lyapin, A. G.; Hemley, R. J. *Philos. Mag.* **2002**, *82*, 231–253.
(3) Kaner, R. B.; Gilman, J. J.; Tolbert, S. H. *Science* **2005**, *308*, 1268–1269.
(4) Gilman, J. J.; Cumberland, R. W.; Kaner, R. B. *Int. J. Refract. Met. Hard Mater.* **2006**, *24*, 1–5.
(5) Levine, J. B.; Tolbert, S. H.; Kaner, R. B. *Adv. Funct. Mater.* **2009**, *19*, 3519–3533.
(6) Chung, H. Y.; Weinberger, M. B.; Levine, J. B.; Kavner, A.; Yang, J. M.; Tolbert, S. H.; Kaner, R. B. *Science* **2007**, *316*, 436–439.
(7) Rau, J. V.; Latini, A. *Chem. Mater.* **2009**, *21*, 1407–1409.
(8) Cumberland, R. W.; Weinberger, M. B.; Gilman, J. J.; Clark, S. M.; Tolbert, S. H.; Kaner, R. B. *J. Am. Chem. Soc.* **2005**, *127*, 7264–7265.
(9) Hao, X.; Xu, Y.; Wu, Z.; Zhou, D.; Liu, X.; Cao, X.; Meng, J. *Phys. Rev. B: Condens. Matter Mater. Phys.* **2006**, *74*, 224112 (1−5).
(10) Chen, X. Q.; Fu, C. L.; Kremar, M.; Painter, G. S. *Phys. Rev. Lett.* **2008**, *100*, 196403 (1−4).
(11) Wang, M.; Li, Y.; Cui, T.; Ma, Y.; Zou, G. *Appl. Phys. Lett.* **2008**, *93*, 101905 (1−3).
(12) Latini, A.; Rau, J. V.; Ferro, D.; Teghil, R.; Rossi Albertini, V.; Barinov, S. M. *Chem. Mater.* **2008**, *20*, 4507–4511.
(13) Rau, J. V.; Latini, A.; Generosi, A.; Rossi Albertini, V.; Ferro, D.; Teghil, R.; Barinov, S. M. *Acta Mater.* **2009**, *57*, 673–681.
(14) Latini, A.; Rau, J. V.; Teghil, R.; Generosi, A.; Rossi Albertini, V. *ACS Appl. Mater. Interfaces* **2010**, *2*, 581–587.
(15) Ivanov, B. L.; Wellons, M. S.; Lukehart, C. M. *J. Am. Chem. Soc.* **2009**, *131*, 11744–11750.
(16) Latini, A.; Gozzi, D.; Di Pascasio, F. *J. Alloys Compd.* **2002**, *346*, 311–316.
(17) *IVTANTHERMO for Windows, database on thermodynamic properties of individual substances, Version 3.0*; Glushko Thermocenter of the Russian Academy of Sciences: Moscow.
(18) Teghil, R.; De Bonis, A.; Galasso, A.; Santagata, A.; Villani, P.; Sordelet, D. J. *Chem. Phys. Lett.* **2007**, *438*, 85–88.
(19) Joensson, B.; Hogmark, S. *Thin Solid Films* **1984**, *114*, 257–269.
(20) Korsunsky, A. M.; McGurk, M. R.; Bull, S. J.; Page, T. F. *Surf. Coat. Technol.* **1998**, *99*, 171–183.
(21) Iost, A.; Bigot, R. *Surf. Coat. Technol.* **1996**, *80*, 117–120.
(22) Iost, A.; Bigot, R. *J. Mater. Sci.* **1996**, *31*, 3573–3577.
(23) *Database JCPDS*; International Centre for Diffraction Data: Newtown Square, PA, 2000.
(24) Okada, S.; Kudou, K.; Lundstrom, T. *Jpn. J. Appl. Phys.* **1995**, *34*, 226–231.
(25) Gu, Q.; Krauss, G.; Steurer, W. *Adv. Mater.* **2008**, *20*, 3620–3626.
(26) Mohammadi, R.; Lech, A. T.; Xie, M.; Weaver, B. E.; Yeung, M. T.; Tolbert, S. H.; Kaner, R. B. *Proc. Natl. Acad. Sci. U.S.A.* **2011**, *108* (27), 10958–10962.
(27) Brazhkin, V.; Dubrovinskaia, N.; Nicol, M.; Novikov, N.; Riedel, R.; Solozhenko, V.; Zhao, Y. *Nat. Mater.* **2004**, *3*, 576–577.
(28) Levine, J. B.; Betts, J. B.; Garrett, J. G.; Guo, S. Q.; Eng, J. T.; Migliori, A.; Kaner, R. B. *Acta Mater.* **2010**, *58*, 1530–1535.
(29) Sundgren, J. E. *Thin Solid Films* **1985**, *128*, 21–44.